Applied Catalysis B: Environmental 324 (2023) 122254

Contents lists available at ScienceDirect

Applied Catalysis B: Environmental

journal homepage: www.elsevier.com/locate/apcatb

The study of Pd-SSZ-13 as low-temperature passive NO_x adsorber materials: High dispersal of Pd in small-pore CHA zeolites by thermal treatment

Yingjie Wang [a,c], Xiaoyan Shi [a,b,*], Zhongqi Liu [a,b], Yulong Shan [a], Wei Shi [a,b], Yunbo Yu [a,b,c], Hong He [a,b,d,*]

[a] State Key Joint Laboratory of Environment Simulation and Pollution Control, Research Center for Eco-Environmental Sciences, Chinese Academy of Sciences, Beijing 100085, China
[b] University of Chinese Academy of Sciences, Beijing 100049, China
[c] Ganjiang Innovation Academy, Chinese Academy of Sciences, Ganzhou 34100, China
[d] Center for Excellence in Regional Atmospheric Environment, Institute of Urban Environment, Chinese Academy of Sciences, Xiamen 361021, China

ARTICLE INFO

Keywords:
Palladium zeolite catalyst
Pd-SSZ-13
Passive NO_x adsorber
Thermal treatment
Palladium transformation

ABSTRACT

In this work, Pd-SSZ-13 catalysts with 1.0 wt% Pd loading were studied as passive NO_x adsorber (PNA) materials. A series of Pd-SSZ-13 catalysts were prepared by calcination of the initially prepared Pd-SSZ-13 under static air following different steps. It was found that, the interaction of PdO_x nanoparticles and $Pd(OH)_2$ with Brønsted acid sites can facilitate the migration of the Pd species from the external surface to inside the crystal and subsequent anchoring on ion-exchange sites during the thermal treatment. The results suggest that the thermal treatment could be a superior means for the preparation of Pd-SSZ-13 with highly dispersed Pd ions, because it causes less degradation of the zeolite framework. The NO_x adsorption/desorption performance of various Pd-SSZ-13 catalysts in the presence of H_2O and under the co-existence of CO and H_2O were studied and compared.

1. Introduction

The stringent regulations for NO_x emission from lean-burn diesel vehicles require after treatment systems with high efficiency. The selective catalytic reduction of NO_x by ammonia (NH_3-SCR) has been widely applied for the removal of NO_x emissions from diesel vehicles. The state-of-the-art NH_3-SCR systems can successfully reduce NO_x at temperatures above 200 °C [1,2]. Meanwhile, the need for further reduction in NO_x emissions from diesel vehicles has been acknowledged by both administrators and manufacturers [2]. For instance, the current NO_x emission standard for EPA 2010 is 0.20 g/bhp-hr, while the California Air Resources Board proposes an ultra-low NO_x emission standard of 0.02 g/bhp-hr for the model year 2024. Generally, the exhaust temperatures in the cold start World Harmonized Transient Cycle (WHTC) are below 200 °C in the first ~1000 s of operation [3]. Therefore, the removal of NO_x emissions from the cold start period is important to meet the increasingly stringent regulations. In recent years, Passive NO_x Adsorbers (PNA), in which NO_x can be stored below 200 °C and then released at higher temperatures, have been considered as a promising strategy for reducing cold-start NO_x emissions [4–6].

Catalysts consisting of Pd supported on oxides (e.g. $CeZrO_x$, CeO_2) and zeolites (e.g. BEA, ZSM-5, SSZ-13) have been studied as PNA materials [6]. Pd-zeolites are among the candidate PNA materials; in particular, the small pore zeolite Pd-SSZ-13 with chabazite structure exhibits high NO_x trapping efficiency and excellent hydrothermal stability [6–9]. Previous reports proposed that highly dispersed Pd^{2+} ions in Pd-zeolites are the active sites for NO adsorption at low temperature [7–10]. In particular, Pd^{2+} ions associated with paired Al sites (denoted as Z_2Pd^{2+}, where Z represents an ion-exchange site) and $Z[Pd^{2+}(OH)]^+$ ions balanced by a single Al site are proposed as NO storage sites, via the formation of Pd^{2+}-NO and Pd^{+}-NO [7–12]. However, it is difficult to achieve highly dispersed Pd ions in SSZ-13 zeolites by common ion exchange methods, possibly due to the diffusion limitation of the small pore size (3.8 Å) of the CHA structure [9,13]. Khivanstev et al. prepared Pd-SSZ-13 with atomically dispersed Pd ions by a modified incipient wetness impregnation method, using NH_4-SSZ-13 with low Si/Al ratio (Si/Al=6) as the parent zeolite [7]. Furthermore, Zhao et al., proposed that the high Pd dispersion owed to the formation of $Pd(NH_3)_x^{2+}$ intermediates in NH_4-SSZ-13 [14]. On the other hand, Yasumura et al. reported the atomic dispersion of bulk Pd to Pd^{2+} cations in CHA zeolites

* Corresponding authors at: State Key Joint Laboratory of Environment Simulation and Pollution Control, Research Center for Eco-Environmental Sciences, Chinese Academy of Sciences, Beijing 100085, China
E-mail addresses: xyshi@rcees.ac.cn (X. Shi), honghe@rcees.ac.cn (H. He).

https://doi.org/10.1016/j.apcatb.2022.122254
Received 18 October 2022; Received in revised form 28 November 2022; Accepted 1 December 2022
Available online 5 December 2022

(Si/Al~6.8) by pretreatment of mixture of Pd black and CHA zeolite under 4% NO flow at 600 °C [15]. Some groups found that the transformation of PdO to isolated Pd ions could occur by thermal or hydrothermal treatment of Pd-zeolites at high temperatures (e.g., 750 °C), improving the PNA performance of the Pd-zeolites[8,10,13,16–18]. The results of Lee and coworkers showed that the redistribution of Pd and the enhancement of the NO storage capacity of Pd-SSZ-13(Si/Al=22.4) can be realized by hydrothermal treatment at 750 °C for 25 h, while thermal treatment exhibited a negligible effect [8,13]. Moreover, Lardinois et al. reported that a fraction of the agglomerated PdO can be transformed to isolated Pd^{2+} ions via thermal treatment of Pd-CHA (Si/Al=12) at 750 °C [17]. On the other hand, the dealumination of the zeolite framework and transformation of Pd species could occur simultaneously during hydrothermal treatment [16,17]. Those results suggest that the dispersion of Pd in zeolites can be influenced by the properties of the parent zeolites (e.g. Si/Al ratio, cation type), the initial state of Pd speciation and the treatment conditions, etc.

The NO_x storage capacity of Pd-SSZ-13 can be inhibited by H_2O, which is a common component in cold-start exhaust from diesel engines [9,11]. Moreover, it has been reported that the PNA performance of Pd/zeolites can be promoted by low-concentration CO, which is also a component in cold-start exhaust [7,18–23]. However, the mechanism of the effect of CO on the PNA performance of Pd-SSZ-13 is still not well understood. Based on IR studies, Khivanstev et al. proposed that the improvement of the PNA performance of Pd-SSZ-13 by CO is attributed to the formation of carbonyl-nitrosyl complexes such as Pd(II)(NO)(CO) [7,19,20]. On the other hand, some groups proposed that the reduction of Pd^{2+} to Pd^{+} by CO could be responsible for the promotion of NO storage by CO [21–23]. Accordingly, further research is needed to investigate the NO_x adsorption/desorption behaviors of Pd-SSZ-13 in the presence of CO.

In this work, a series of Pd-SSZ-13 catalysts with different predominant Pd species was obtained by thermal or hydrothermal treatment of the same initial Pd-SSZ-13 sample, in which the majority of Pd was in the form of PdO_x. The NO_x adsorption/desorption behaviors and PNA performance of thermally treated Pd-SSZ-13 were extensively investigated and compared with those of hydrothermally treated samples. The objective of this work is to investigate the distribution mechanism of Pd species during the thermal treatment process and identify the Pd sites for NO_x adsorption in Pd-SSZ-13, as well as the effect of CO on different Pd sites. Additionally, the effects of thermal and hydrothermal treatment on the catalytic performance of Pd-SSZ-13 were compared. In particular, the role of Brønsted acid sites on the anchoring and migration of the Pd species in SSZ-13 during high-temperature thermal treatment was elucidated.

2. Experimental methods

2.1. catalysts preparation

Tetraammine palladium (II) nitrate solution (Sigma-Aldrich) was used as the Pd precursor. NH_4-SSZ-13 with ratio of Si/Al= 7.6 was ion-exchanged in a solution containing 1.0 wt% Pd to the parent zeolite for 24 h at 65 °C, and then the slurry was transferred to a rotary evaporator to remove the water. In this way, the possibility of Pd loss during the washing process typical of the ion-exchange method can be avoided. The Pd-SSZ-13 sample with 1.0 wt% Pd was dried at 80 °C overnight as the initial sample, and subsequently calcined in static air according to different calcination processes. The Pd-SSZ-13 calcined at 500 °C for 2 h with a ramp rate of 1 °C/min was denoted as Pd-500. Two Pd-SSZ-13 catalysts were calcined following a two-step calcination process: the same calcination process of Pd-500 followed by further calcining at 750 °C for 2 h or 750 °C for 24 h. The obtained samples were named Pd-750 and Pd-TA, respectively. In addition, Pd-HTA was prepared by hydrothermal aging of Pd-500 at 750 °C in 10% H_2O/air for 24 h. Moreover, the parent H-SSZ-13 was subjected to thermal or hydrothermal aging under the same TA or HTA conditions, denoted as H-SSZ-13-TA and H-SSZ-13-HTA, respectively. In this paper, the TA and HTA treatments represent the thermal aging and hydrothermal aging treatment of samples at 750 °C for 24 h.

2.2. Catalyst characterization

The metallic element contents of the catalysts were analyzed using Inductively Coupled Plasma Optical Emission Spectrometry (ICP-OES, Varian 720).

Powder X-ray diffraction (XRD) measurements were carried out on a Bruker D8 Advance diffractometer with Cu Kα radiation (40 kV, 30 mA and $\lambda = 0.15406$ nm). The XRD patterns were recorded in the range from 4° to 45° with a step size of 0.02°. The relative crystallinity of each aged sample was assessed according to the peak intensity within the range of $25^\circ \leq 2\theta \leq 33^\circ$ by using the corresponding fresh sample with 100% crystallinity as the baseline.

Solid-state ^{27}Al and ^{29}Si MAS NMR spectra were collected on a JNM-ECZ600R Solid-State NMR spectrometer, with a spectral window of 156 MHz (Al) using a 3.2 mm MAS probe or 119 MHz (Si) using a 3.2 mm MAS probe. A relaxation delay of 5 s for Si and Al was applied to collect single-pulse spectra. TMS and $AlCl_3$ were used as external references, respectively.

The H_2-TPR experiments were carried out on a Micromeritics AutoChem 2920 chemisorption analyzer. The catalysts (50 mg) were pretreated at 500 °C in a flow of O_2/He (50 mL/min) for 1 h then cooled down to − 50°C and recorded as dehydrated. The hydrated samples were purged in Ar for 30 min without pretreatment. H_2-TPR was performed in 10 vol% H_2/Ar gas flow at 50 mL/min and the temperature was ramped linearly from − 50°C to 400 °C at a heating rate of 10 °C /min.

The morphology, mean size and dispersion of the Pd particles spread on the samples were investigated by Transmission Electron Microscopy (TEM). These analyses were performed using a JEOL JEM-2100 F microscope, operating at 200 kV.

The X-ray photoelectron spectroscopy (XPS) experiments were performed on a photoelectron spectrometer (Axis Ultra, Kratos Analytical Ltd.) with Al Kα radiation (1486.6 eV) as the primary excitation. Binding energies were calibrated on the basis of the C 1 s peak at 284.6 eV.

FTIR spectra between 3200 and 4000 cm^{-1} were recorded with a Nicolet iS50 spectrometer. The sample (20 mg) was pressed into thin sheets at 3–4 MPa pressure and placed in a vacuum chamber on a homemade bracket. In a typical experiment, sample slices were first pretreated at 500 °C in a vacuum for 1 h to remove moisture. The sample was then cooled down to 120 °C in a vacuum and the spectrum was recorded when it reached stability.

NH_3 temperature programmed desorption (NH_3-TPD) measurements were conducted to investigate the acidity of catalyst samples. Around 120 mg of sample was placed into the quartz tube and pretreated at 500 °C in 20% O_2/N_2 for 30 min, then cooled to 120 °C and purged in N_2 for 1 h. The NH_3 adsorption was carried out under a gas flow of 500 ppm NH_3/N_2 at 120 °C until saturated. After that, the NH_3 flow was turned off and the sample was purged in N_2 for 1 h until the NH_3 signal was undetectable. The NH_3 desorption process was conducted from 120 to 600 °C with a ramp rate of 10 °C/min. The concentrations of NH_3 were continually monitored by a Nicolet iS50R FTIR spectrometer with a multiple path gas cell (2 m).

2.3. NO_x adsorption/desorption experiments

Conventional PNA experiments were performed using 40–60 mesh particulate samples in a fixed-bed quartz flow reactor at atmospheric pressure. Approximately 75 mg of sample was packed in a quartz tube and tested with a total flow rate of 250 mL/min feed gas containing 200 ppm NO, 200 ppm CO (if used), 5% H_2O, 10% O_2, balance N_2, GHSV≈ 150,000 h^{-1}. Concentrations of reactants and products were measured by an ANTARIS IGS online gas analyzer. Although it is preferable to use

pure NO as feed gas in the study, the actual feed gas contained about 200 ppm of NO and about 10 ppm of NO_2 coming from the oxidation of NO in the heated gas pipeline. Since realistic engine exhaust does contain around 5% NO_2, no attempt was made to remove NO_2 from our feed gas. Before the NO_x adsorption test, the samples were pretreated in 10% O_2 and 5% H_2O, balanced in N_2 flow at 500 °C for 30 min, then cooled to 120 °C in the same feed gas. Then 210 ppm of NO_x was introduced to the mixture. After stabilization, the sample adsorbed NO_x for 10 min at 120 °C and was then heated from 120 °C to 700 °C at a rate of 10 °C/min while the composition of the outlet gas was recorded.

The NO_x temperature programmed desorption (NO_x-TPD) was performed using 150 mg of catalyst under the same feed gas as the PNA experiments. After NO_x adsorption for 10 min at 120 °C, the catalyst was purged by feed gas without NO for 1 h, and then the TPD experiment was conducted from 120 °C to 700 °C with a heating rate of 10 °C/min. The remaining pretreatment and desorption steps were consistent with those of the conventional NO_x adsorption tests.

3. Results and discussion

3.1. Textural properties of Pd-SSZ-13 catalysts

In this work, the Pd-SSZ-13 catalysts, which were denoted as Pd-500, Pd-750, Pd-TA and Pd-HTA, were prepared from the same initial Pd-SSZ-13 sample with ~1.0 wt% Pd loading (the BET surface areas and pore volumes as well as the Si/Al ratios of Pd-SSZ-13 and the parent SSZ-13 are summarized in Table S1). There was no Pd loss after thermal or hydrothermal treatment. The Pd/Al ratio was ~0.054 for those samples.

The XRD results of H-SSZ-13 and Pd-SSZ-13 catalysts are shown in Fig. 1. It can be seen that all test samples exhibited the XRD pattern of the CHA structure. Although the zeolite framework of Pd-SSZ-13 was well-maintained after hydrothermal or thermal aging, a slight decrease in the intensity of the diffraction peaks was observed for Pd-TA and Pd-HTA. Compared to Pd-500, the Pd-TA and Pd-HTA samples retained relative crystallinities of ~88% and 85%, respectively. Moreover, as shown by the magnified region of 30–34.5° in Fig. 3(b), the XRD patterns of Pd-TA and Pd-HTA shifted to higher angles, indicating a contraction of the lattice after hydrothermal or thermal aging [16]. Pd-HTA showed a more significant angle shift and decline in signal intensity than Pd-TA. This suggests that the hydrothermal aging of Pd-SSZ-13 in steam can cause more severe structure degradation compared to thermal aging in dry air. The PdO in Pd-zeolites could exhibit a diffraction peak at ~33.9° (JCPDS 43–1024) [10]. However, it is difficult to clarify the nature of PdO in the Pd-SSZ-13 samples by XRD. As shown in Fig. 1(b), just a very weak peak at ~33.9° could be observed in the patterns of Pd-750 and Pd-HTA. In addition, both hydrothermal and thermal aging can result in structure degradation of the parent H-SSZ-13, as the magnified XRD patterns in the region from 22 to 34.5° show in Fig. S1.

Solid-state ^{27}Al NMR was conducted to investigate the changes in the local Al environment in the zeolite framework of H-SSZ-13 and Pd-SSZ-13 samples. As shown in Fig. 2, the parent H-SSZ-13 and Pd-500 exhibit strong resonances arising from the four-coordinate framework Al at a chemical shift of ~ 58 ppm [24–27]. A decline in the signal intensity of the peak for framework Al at ~58 ppm can be observed for Pd-750, indicating the occurrence of framework dealumination for the synthesized Pd-SSZ-13 after calcination at 750 °C for 2 h. Further thermal treatment results in more serious framework dealumination, as shown by the results of Pd-TA. As expected, the hydrothermally aged Pd-HTA exhibits a decrease in the intensity of the peak for framework Al at ~58 ppm. It should be noted that Pd-TA remained more framework Al compared with Pd-HTA, in accordance with the common knowledge that hydrothermal aging can accelerate the dealumination of zeolites, due to the hydrolysis of Si-OH-Al [24–27]. In addition, as shown by the ^{27}Al NMR spectra in Fig. 2, hydrothermal aging can cause more serious dealumination of the zeolite framework for H-SSZ-13 compared with Pd-SSZ-13. We assume that the Pd species at the ion-exchange sites of zeolites can protect the framework Al, similar to the case of Cu-SSZ-13, in which copper exchanged into SSZ-13 can enhance the thermally stability and stabilize the framework Al during hydrothermal aging [24, 26,28]. Moreover, the initial H-SSZ-13 product contained a certain amount of extra-framework Al, as evidenced by the broad resonance centered at ~0 ppm [27]. According to the ^{29}Si MAS NMR spectra (Fig. S2), the Si/Al ratio of the zeolite framework of H-SSZ-13 was calculated as ~8.2, which was higher than the Si/Al ratio of ~7.6 derived from ICP analysis. This further confirms the existence of

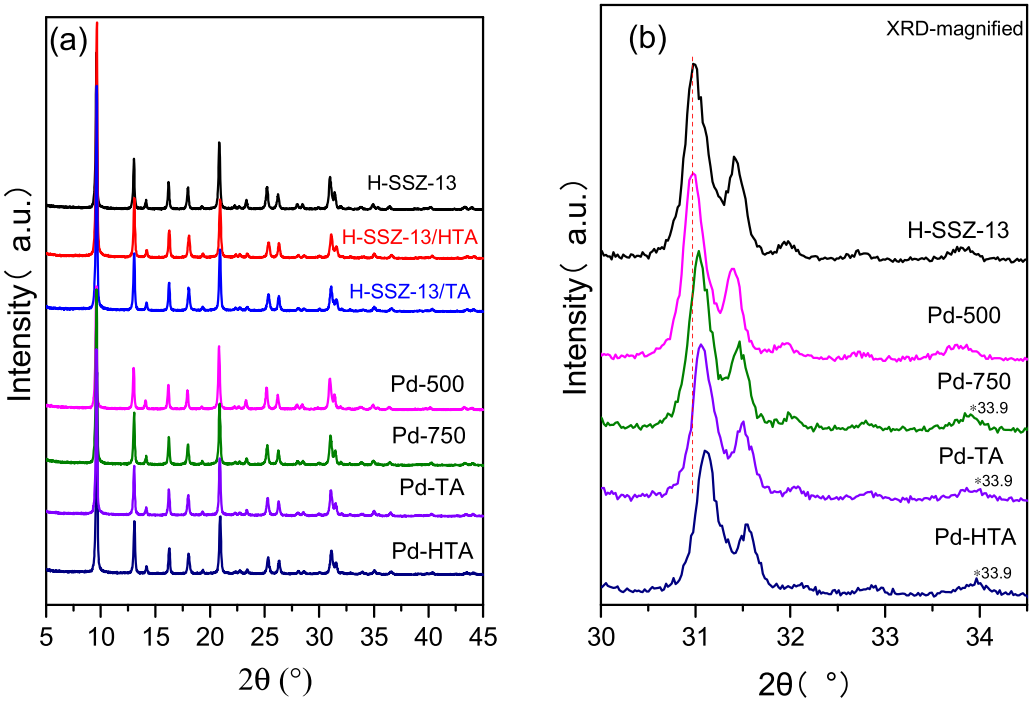

Fig. 1. (a) XRD patterns of Pd-SSZ-13 catalysts and H-SSZ-13 zeolites, (b) enlarged XRD patterns in the 30–34.5° region.

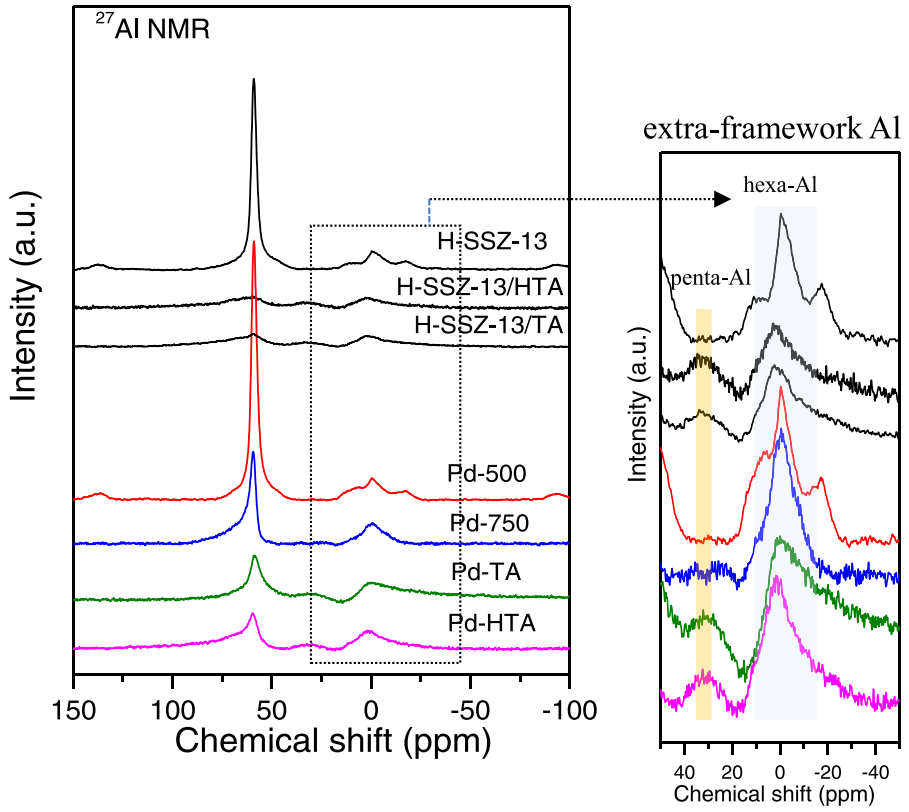

Fig. 2. Solid state ^{27}Al MAS NMR spectra of Pd-SSZ-13 catalysts and H-SSZ-13 zeolites.

extra-framework Al in our samples. As shown in the enlarged view of the chemical shift range from − 40 to + 40 ppm to the right in Fig. 2, a resonance centered at ~30 ppm related to penta-Al appeared for all TA and HTA samples, which further confirms the dealumination of the zeolites [13,24,25,27].

3.2. The state and dispersion of Pd in Pd-SSZ-13

H_2-TPR experiments were used to identify the Pd species in zeolites. According to the literature, the reduction of PdO to Pd could result in H_2 consumption in the temperature range from 5 to 25 °C during the H_2-TPR of Pd-zeolites [10,13,16,17,29,30]. A small H_2 release peak at ~ 60–70 °C could usually be observed due to the decomposition of PdH_x formed during the reduction of PdO to metal Pd [10,17,29,30]. Additionally, the reduction of Pd^{2+} ions to metallic Pd in zeolites could exhibit a broad feature in the temperature region from 90°C-250°C, and the desorption of Ar physisorbed within the zeolite could contribute to the H_2 consumption below − 10 °C [10,11,16,17,30]. As shown by the H_2-TPR profiles in Fig. 3(a), H_2 consumption peaks from the desorption of Ar can be observed in the range from − 50 to − 15°C, while H_2 consumption peaks related to the reduction of Pd^{2+} ions to metallic Pd are difficult to identify in our work. This might be explained by the oxidative pretreatment at 500 °C for 30 min resulting in the dehydration of Pd-SSZ-13 samples, in which the reduction of Pd^{2+} ions showed broad features with a weak signal and was difficult to accurately quantify [10,17,29].

Therefore, in this work, only the PdO species in Pd-SSZ-13 were quantified based on the H_2 consumption between 5 and 25 °C, and the H_2 release from the decomposition of PdH_x was subtracted. Based on this, the H_2 consumption from the reduction of PdO to metal Pd was

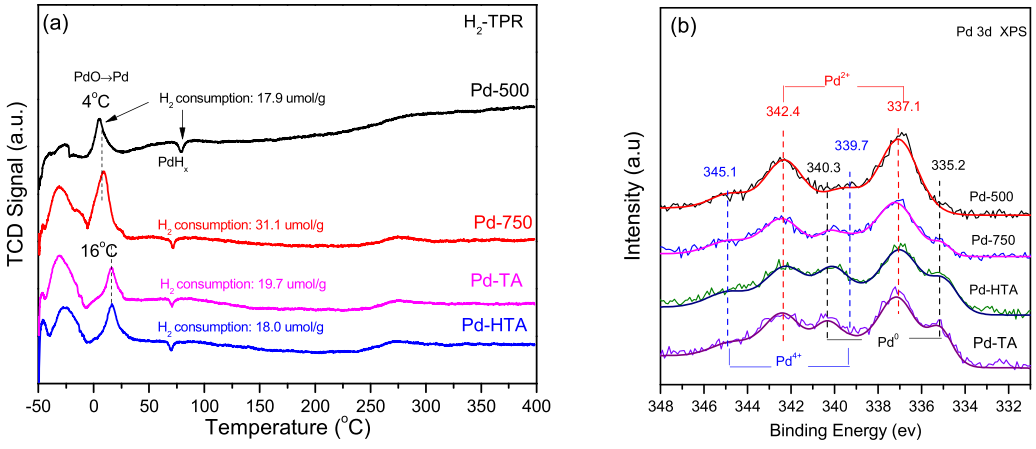

Fig. 3. (a) H_2-TPR profiles of Pd-SSZ-13 catalysts, (b) XPS profiles of a series of Pd-SSZ-13 catalysts.

calculated and shown in Fig. 3(a). It can be seen that Pd-750 contains more PdO compared with Pd-500, indicating that Pd^{2+} ions agglomerated during TA treatment at 750 °C for 2 h. Interestingly, the amount of PdO in Pd-TA was decreased, indicating the transformation of PdO to Pd ions during TA treatment for 24 h. Moreover, compared with Pd-500, the reduction peaks of smaller-size PdO particles in Pd-TA and Pd-HTA appeared at higher temperatures. A similar phenomenon had also been observed by some groups [13,29]. Such shift in the reduction peaks to higher temperature can be explained by two reasons: (1) after HTA and TA treatment, the PdO particles migrated into the inner part of the zeolite crystal according to the results of XPS, (2) the dealumination of Pd-TA and Pd-HTA increased the amount of extra-framework Al (evidenced by NMR results), resulting in the interaction of small PdO particles with extra-framework Al [31]. These results suggest that the re-dispersion of larger PdO_x particles to Pd^{2+} ions and smaller PdO_x particles could take place after TA or HTA treatment at 750 °C for 24 h [10].

The chemical states of Pd species in the Pd-SSZ-13 samples were analyzed by XPS and the Pd3d spectral curves are shown in Fig. 3(b). According to the literature [9,13,17,30], the high-intensity peaks at 337.1 eV (Pd $3d_{5/2}$) and 342.4 eV (Pd $3d_{3/2}$) could be assigned to the Pd^{2+} in Pd-SSZ-13. The weak peaks at 339.7 eV (Pd $3d_{5/2}$) and 342.4 eV (Pd $3d_{3/2}$) could be attributed to Pd^{4+}, and the peaks at 335.2 eV (Pd $3d_{5/2}$) and 340.2 eV (Pd $3d_{3/2}$) could be assigned to Pd^0, respectively [9,30]. As shown by the results in Fig. 3(b), Pd-750, Pd-TA and Pd-HTA exhibited lower intensity palladium 3d XPS signals compared to Pd-500, indicating that the migration of Pd species in Pd-SSZ-13 deeper inside the zeolite crystallites could be partially facilitated by TA and HTA treatment at 750 °C [13,17]. Furthermore, the state of Pd in these samples is dominated by divalent Pd, and the signal of Pd^{4+} can be detected, indicating the existence of PdO_2. However, PdO_2 was hard to identify by H_2-TPR, since the H_2 consumption from the reduction of PdO_2 might overlap with the reduction of PdO. It is worth noting that a prominent signal for metallic Pd can be observed at 335.2 eV ($3d_{5/2}$) for Pd-TA and Pd-HTA. We assume that the decomposition of PdO to metallic Pd occurred during TA and HTA treatment, and the few well-distributed metallic Pd could not be re-oxidized to PdO during the cooling process and remained in the Pd-TA and Pd-HTA samples.

The dispersion of Pd in SSZ-13 was further investigated by TEM analysis. As shown by the TEM image of Pd-500 in Fig. 4(a), the distribution of Pd particles on SSZ-13 crystals was relatively broad, with an average particle size of 3.8 ± 1.1 nm as determined by counting approximately 100 isolated particles. After calcination at 750 °C for 2 h, the Pd particles transformed to smaller sizes (< 3 nm) and the dispersion of Pd became more homogenous, as shown by the image of Pd-750 in Fig. 4(b). Furthermore, only small numbers of nanoparticles (1–2 nm) can be observed in the Pd-TA and Pd-HTA samples, as shown in Fig. 4(c) and (d). This indicates that the majority of Pd in Pd-TA and Pd-HTA is highly dispersed [7], in good agreement with the results of H_2-TPR analysis.

3.3. The Pd distribution during thermal treatment

NH_3-TPD and FTIR were used to investigate the acid sites of H-SSZ-13 and Pd-SSZ-13 samples. As shown by the NH_3-TPD profiles in Fig. 5 (a), H-SSZ-13 exhibits a high-intensity peak at temperatures above 350 °C related to NH_3 desorption from strong Brønsted acid sites, where the NH_3 desorption below ~220 °C can be assigned to weak acid sites associated with extra-framework Al [24–26,30]. It can be seen that the Brønsted acid sites of Pd-500 were only slightly decreased compared with the parent H-SSZ-13. Moreover, the TA treatment at 750 °C resulted in a marked reduction in the number of the Brønsted acid sites, as the results for Pd-750 and Pd-TA illustrate. The HTA treatment also resulted in a decrease in the number of Brønsted acid sites, as shown by the results for Pd-HTA. Additionally, an increase in NH_3 desorption between 200 and 320 °C can be observed on Pd-750, Pd-TA and Pd-HTA, derived from Pd sites [25,30,32,33].

Fig. 5(b) compares the transmission FTIR spectra in the -OH stretching region for the tested samples. The parent H-SSZ-13 exhibits bands at 3732 cm^{-1} and 3610 cm^{-1}, which can be assigned to Si-OH groups and bridging Si(OH)Al groups (Brønsted acid sites), respectively [12,26,34–37]. The band at 3660 cm^{-1} can be assigned to Al-OH groups (extra-framework Al), while the band at 3583 cm^{-1} can be assigned to H-bonded Si-OH groups. Compared to the parent H-SSZ-13, no detectable change in the peak for Si(OH)Al (~3610 cm^{-1}) but a slight decrease in the peak corresponding to Al-OH groups (~3660 cm^{-1}) can

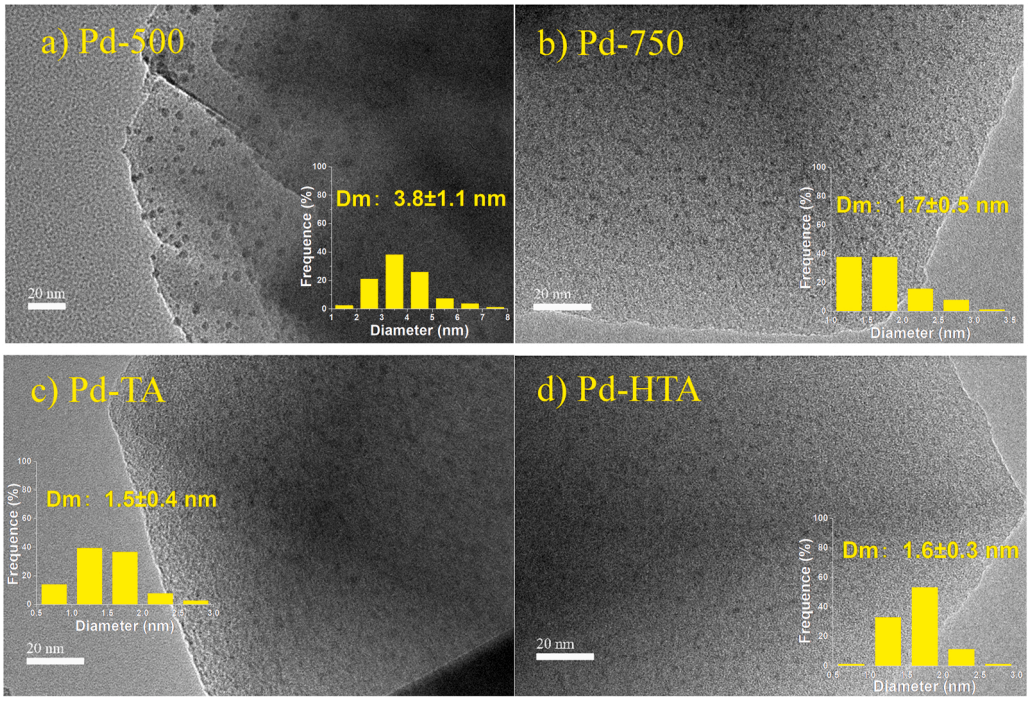

Fig. 4. TEM images of Pd-500 (a), Pd-750 (b), Pd-TA (c), Pd-HTA (d).

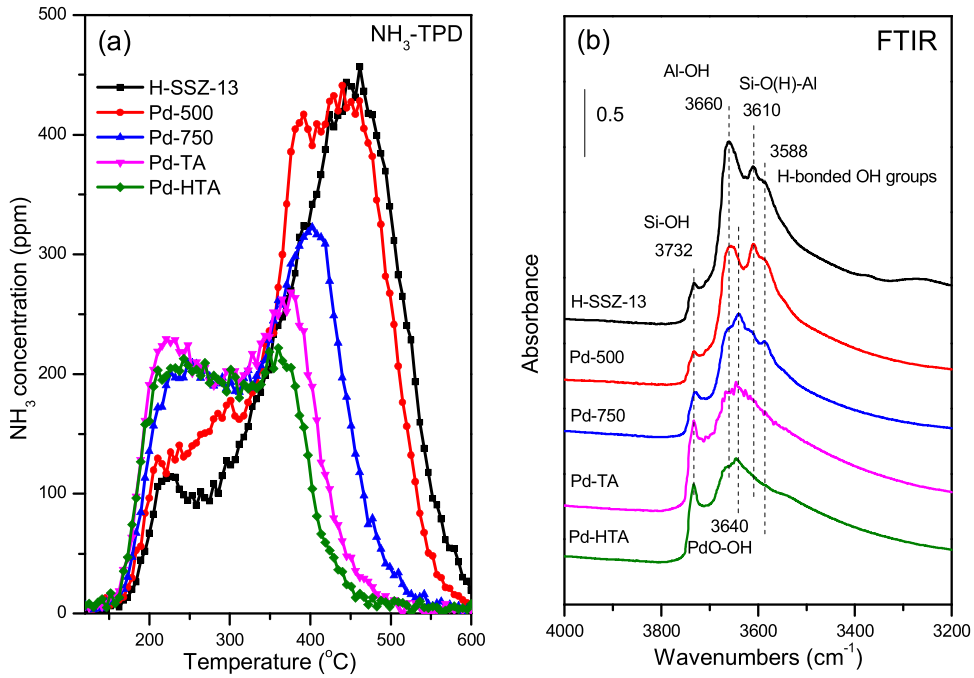

Fig. 5. (a) NH_3-TPD profiles of the series of samples, (b) Transmission IR spectra of samples under vacuum.

be detected for Pd-500. After further calcination at 750 °C, a marked decrease in the Brønsted acid peak (3610 cm^{-1}) could be observed on Pd-750 and Pd-TA, indicating the consumption of Brønsted acid sites.

The Brønsted acid sites (Si(OH)Al) in zeolites are important for anchoring PdO species and forming Pd^{2+} ions via "protonolysis", in which the PdO particles react with the protons in zeolites according to reaction R(1) [9,12,22,34,38,39]. Brønsted acid sites are abundant in the Pd-500 sample, according to the results of NH_3-TPD. Therefore, PdO in Pd-500 can diffuse into the zeolite pores during TA treatment via R (1). Furthermore, similar to the conversion of Z-$[Cu^{2+}(OH)]^+$ to Z_2-Cu^{2+} or CuO_x in Cu-SSZ-13 during hydrothermal aging, the Z-$[Pd^{2+}(OH)]^+$ in Pd-SSZ-13 might possibly convert to Z_2-Pd^{2+} or PdO_x during TA or HTA treatment, of which Z_2-Pd^{2+} sites are more thermodynamically stable than Z-$[Pd^{2+}(OH)]^+$ [17,36,40]. Moreover, $Pd(OH)_2$ can be possibly formed during calcination of the initial Pd-SSZ-13 product in static air at 500 °C [15]. The mobile $Pd(OH)_2$ intermediates can participate in the migration and transformation of Pd in zeolites, as illustrated by reactions R(2) to R(4) [13,14,24,36,40]. After thermal treatment of Pd-500 at 750 °C for 2 h, the $Pd(OH)_2$ could convert to small PdO particles and Pd^{2+} ions, which anchor on ion-exchange sites as Z-$[Pd^{2+}(OH)]^+$ and Z_2-Pd^{2+}, according to reactions R(2) to R(4) [24,31,36]. Additionally, the $Pd(OH)_2$ could also interact with hydroxyl groups on extra-framework Al, as evidenced by the marked decrease in the intensity of the band at 3660 cm^{-1} [31].

$$PdO + 2Z\text{-}H^+ \rightarrow 2Z\text{-}Pd^{2+} + H_2O \quad (1)$$

$$Pd(OH)_2 + H^+\text{-}Z \rightarrow Z\text{-}[Pd(OH)]^+ + H_2O \quad (2)$$

$$Pd(OH)_2 + 2H^+\text{-}Z \rightarrow 2Z\text{-}Pd^{2+} + H_2O \quad (3)$$

$$Pd(OH)_2 + Pd(OH)_2 \rightarrow 2PdO + 2H_2O \quad (4)$$

Lee and Ryou et al. reported that the redistribution of Pd species in zeolites can be realized after HTA at 750 °C for 25 h; thus, the NO_x adsorption capacity of Pd-SSZ-13 was significantly enhanced [8,13]. In their study, the presence of H_2O is necessary for the redistribution of PdO particles to ion-exchanged Pd ions, via the hydrolyzation of PdO nanoparticles according to R(5) and then following R(2) and R(3), while thermal treatment at 750 °C for 25 h without H_2O showed negligible effect [8,13]. Contrarily, in our work, a nearly homogenous Pd distribution was realized in CHA zeolites by thermal treatment of Pd-500 at 750 °C for 24 h. We infer that the fact that Pd-500 contained abundant Brønsted acid sites could be mainly responsible for this.

$$PdO + H_2O \rightarrow Pd(OH)_2 \quad (5)$$

It is worth nothing that a new band at 3640 cm^{-1} appeared on Pd-750, and the peak intensity slightly decreased in the spectra of the Pd-TA and Pd-HTA. Some groups reported that the PdO can be anchored on Brønsted acid sites as $Z^-H^+(PdOH)^+Z^-$ [32,33,39]. According to H_2-TPR, Pd-750 contained a relatively larger amount of PdO than other samples. Therefore, we consider that the band at 3640 cm^{-1} could be associated with the O-H stretch from $Z^-H^+(PdOH)^+Z^-$.

On the other hand, the TA or HTA treatment of Pd-500 also resulted in a decrease in the peak intensity of bands related to hydroxyl groups of extra-framework Al (3660 cm^{-1}), indicating the consumption of hydroxyls associated with extra-framework Al [40]. Furthermore, the increasing intensity of the band of Si-OH (3732 cm^{-1}) after TA or HTA treatment could be attributed to isomorphous substitution during the dealumination of the framework, as supported by the results of ^{29}Si NMR (Fig. S2) [27,37].

3.4. NO storage and desorption performance of Pd-SSZ-13

It has been recognized that NO can be stored on isolated Pd^{2+} sites in Pd-SSZ-13 with a molar ratio of 1:1 via the formation of nitrosyl Pd complexes (Pd^{2+}-NO/Pd^{+}-NO) [7,11,13,22]. First, the NO storage performance of Pd-SSZ-13 catalysts was identified by NO_x-TPD experiments after NO_x adsorption at 120 °C in the presence of 5% H_2O. It was found that only a few ppm of NO_2 was detected during NO_x-TPD (Fig. S3). Therefore, the desorption of NO and NO_2 are investigated separately in this work. As shown by the results in Fig. 6(a), Pd-TA and Pd-HTA exhibit markedly higher NO desorption than Pd-500 and Pd-750. Furthermore, the NO desorption features of the Pd-SSZ-13 samples are quite different. For Pd-TA and Pd-HTA, two distinct NO desorption features can be observed in the low- (150–300 °C) and high- (300–450 °C) temperature regions respectively. However, the high-temperature desorption feature made the main contribution to NO desorption from Pd-500 and Pd-750. It has been proposed that

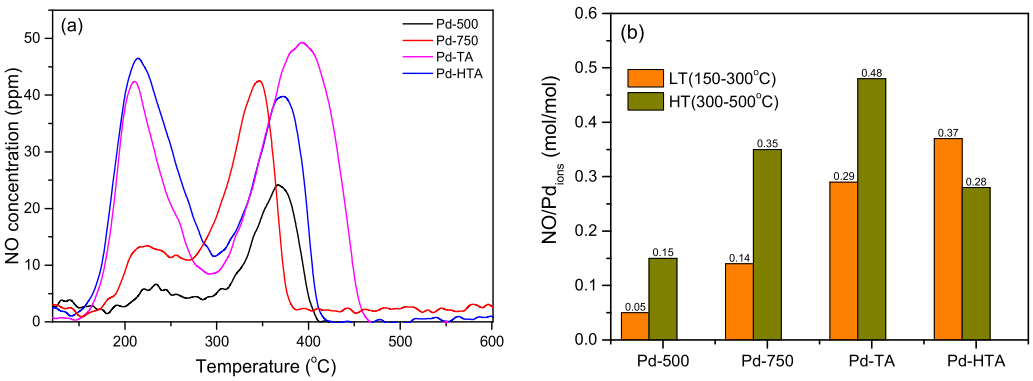

Fig. 6. (a) NO-TPD profiles of various Pd-SSZ-13 catalysts, (b) NO/Pd $_{ions}$ ratios.

Z-$[Pd^{2+}(OH)]^+$ sites can store NO as Pd^+-NO according to reaction (6), while Z_2-Pd^{2+} sites can store NO as Pd^{2+}-NO via R(7) [9,22,41]. The higher desorption temperature of Pd^+-NO than Pd^{2+}-NO might be attributed to the stronger binding of the former [11,41,42]. In the presence of H_2O, the Pd ions in Pd-SSZ-13 might become hydrated at low temperatures, and H_2O-solvated Pd-NO complexes can be formed during NO adsorption on Pd-SSZ-13 in the presence of H_2O [16,17,36,43,44]. Moreover, Song et al. [43] and Gu et al. [44] proposed that, during the TPD process, H_2O can desorb from hydrated Pd nitrosyl complexes prior to NO. Therefore, the low-and high-temperature NO desorptions can be assigned to Pd^{2+}-NO and Pd^+-NO, respectively, while the former should mainly exist as hydrated Pd^{2+}-NO complexes at low temperatures below 200 °C. Furthermore, this speculation can be supported by the situ DRIFTS study of Pd-TA (section "in situ DRIFTS study" in the supporting information).

$$2Z\text{-}[Pd(OH)]^+ + 3NO \rightarrow 2Z\text{-}Pd^+\text{-}NO + NO_2 + H_2O \quad (6)$$

$$Z_2\text{-}Pd^{2+} + NO \rightarrow Z_2\text{-}Pd^{2+}\text{-NO} \quad (7)$$

NO has difficulty adsorbing on PdO or metal Pd nanoparticles [7,31,41,42,45,46], while the small PdO_x nanoparticles in Pd-SSZ-13 might also contribute to the NO_x storage capacity via the formation of Pd-nitrates as indicated in R(8) [8,9,25]. NO_2 should be the main product from the decomposition of Pd-nitrates [19,25]. For our samples, a very small amount of NO_2 could be detected during the desorption stage (Fig. S3), even for Pd-750 with a large amount of PdO. Therefore, we consider that the contribution of PdO_x to the NO storage capacity of these Pd-SSZ-13 samples is negligible.

$$PdO_2 + 2NO + O_2 \rightarrow Pd(NO_3)_2 \quad (8)$$

The amount of Pd^{2+} ions can be estimated by subtracting the amount of PdO_x from total Pd according to the results of H_2-TPR [29]. Since the majority of Pd species in these Pd-SSZ-13 samples are in the bivalent state and just a small amount of metal Pd can be detected according to the XPS results (Fig. 3(b)), we consider that the quantification of Pd^{2+} ions in Pd-SSZ-13 according to the H_2-TPR results is reasonable and acceptable. Considering that NO is primarily stored on isolated Pd ions with a molar ratio of 1:1, the theoretical NO storage capacity of Pd-SSZ-13 should be equivalent to the molar quantity of Pd^{2+} ions in the catalyst. Thus, as shown in Table 1, the ratio of NO/Pd_{ions} is calculated according to the NO desorption amount in the low-temperature (LT) region at 150–300 °C and high-temperature (HT) region at 300–450 °C, respectively. As shown in Fig. 6(b), the NO_x storage capacity of Pd-500 was quite low, with NO/Pd_{ions} ratios of 0.05 and 0.15 for LT and HT, respectively. Calcination at higher temperature (750 °C for 2 h) led to an increase in the number of NO storage sites, so that the total NO/Pd_{ions} of Pd-750 increased to 0.49, of which ~72% was attributed to HT NO desorption. Furthermore, the TA treatment led to a significant increase in the number of NO storage sites, so that the NO/ Pd_{ions} ratios for LT and HT of Pd-TA increased to 0.29 and 0.48, respectively. As expected, the NO storage capacity of Pd-500 could be improved by hydrothermal aging, so that the total NO/Pd_{ions} ratio for Pd-HTA was 0.65 [8,13]. According to the literature [11,22,41], the NO stored on Z_2-Pd^{2+} sites as Pd^{2+}-NO could make the main contribution to NO desorption below ~ 300 °C, while the NO stored on reduced Z-$[Pd^{2+}(OH)]^+$ as Pd^+-NO could contribute to NO desorption above ~ 300 °C. As shown by the results in Fig. 7, Pd-TA exhibited higher HT NO desorption but lower LT NO desorption compared with Pd-HTA. This indicates that Pd-TA contained more Z-$[Pd^{2+}(OH)]^+$ sites while Pd-HTA contained more Z_2-Pd^{2+}sites, in accordance with the results in Fig. 5(c). For Pd-500 and Pd-750, the NO storage capacity is mainly attributed to HT NO desorption, indicating that Pd^+-NO species predominated in these samples. The NO-TPD results further confirmed the re-dispersion of Pd into the zeolite pores and subsequent anchoring on ion-exchanged sites during TA and HTA treatment.

Table 1
Quantification of NO storage capacity (umol/g) on Pd-SSZ-13 samples.

Samples	NO storage capacity (umol/g)				
	without CO[a]			with CO[b]	theoretical storage capacity on Pd ions[c]
	LT (150–300 °C)	HT (300–450 °C)	total	total	
Pd-500	4.0	11.5	15.5	–	76.1
Pd-750	8.5	21.7	30.2	82.2	62.8
Pd-TA	21.5	35.8	57.3	94.1	74.3
Pd-HTA	27.9	20.9	48.8	86.1	75.9

[a] based on the NO-TPD results in Fig. 7(a).
[b] based on the NO-TPD results in Fig. 8.
[c] based on NO: Pd^{2+} ions with a 1:1 mol ratio, in which Pd^{2+} ions were estimated according to H_2-TPR.

It is worth mentioning that the NO/Pd $_{ions}$ ratios are much lower than the theoretical value and are quite different for those samples (Table 1). In the presence of H_2O, NO can adsorb on Z_2-Pd^{2+} sites in the form of hydrated Pd-nitrosyl complexes (Fig. S4) [22,43,44]. Therefore, the Pd-TA and Pd-HTA samples containing more Z_2-Pd^{2+} sites exhibited higher NO storage capacity than Pd-750 and Pd-500. Lee et al. reported that Pd-SSZ-13 became more hydrophobic after hydrothermal treatment at 750 °C, and thus the formation of hydrated Pd ions was suppressed [16]. According to the NMR results (Fig. 2), both TA and HTA treatment caused serious dealumination of Pd-SSZ-13, indicating the increasing hydrophobicity of Pd-TA and Pd-HTA. Therefore, although there is not much difference between the amounts of Pd ions in the Pd-SSZ-13 samples, the NO/Pd ion ratio was different for each sample, due to the difference in the predominant Pd ions sites and hydrophobicity of the zeolites.

As shown above, the NO storage capacity of Pd-SSZ-13 could be improved by TA or HTA treatment. However, even for Pd-TA with highly

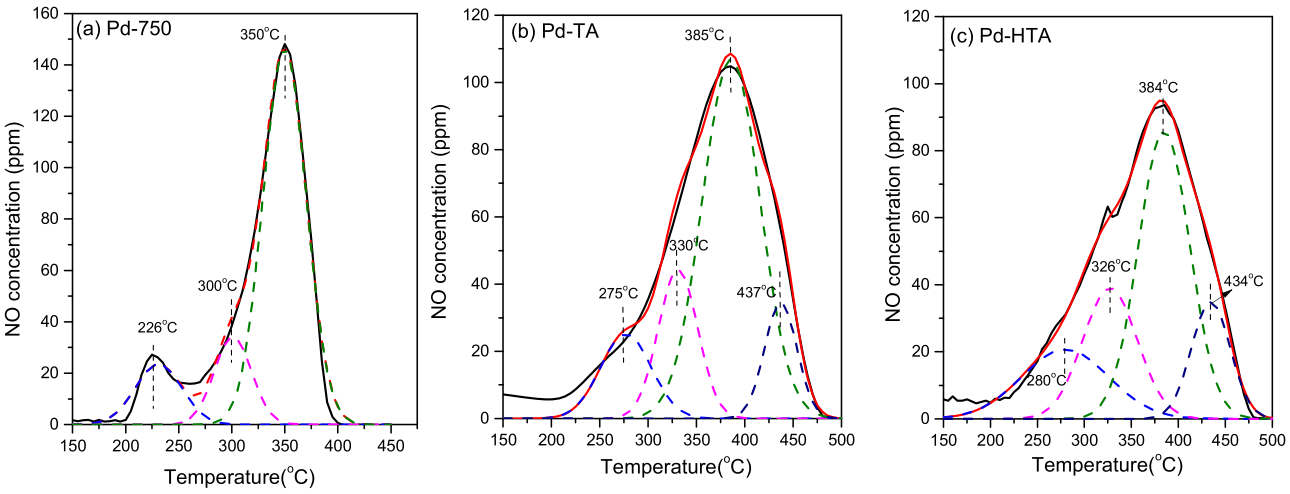

Fig. 7. NO-TPD profiles of various Pd-SSZ-13 catalyst after NO_x adsorption with CO.

dispersed isolated Pd^{2+} ions, the NO/Pd $_{ions}$ ratio is still lower than the theoretical value of ~1. The presence of H_2O (~5%) in the gas feed should inhibit the NO storage, due to the coordination of H_2O on Pd^{2+} ions [19,22]. It has been reported that the inhibition of NO adsorption of Pd-zeolites by H_2O can be suppressed by the addition of low-concentration CO to the gas feed [20,21]. Here, Pd-750, Pd-TA and Pd-HTA were chosen to further investigate the NO_x storage performance under the co-existence of ~200 ppm CO in the feed. As shown by the results in Table 1, the NO storage capacity of the tested Pd-SSZ-13 catalysts was significantly enhanced by CO. If all Pd in Pd-SSZ-13(1.0 wt% Pd) are fully utilized, the NO storage capacity should be estimated as ~ 94.3 umol/g, according to the theoretical ratio of NO storage to total Pd of 1:1. The results show that in the presence of CO, the majority of Pd in Pd-SSZ-13 became active for NO storage. The ratio of NO/Pd_{total} is ~1.00 for Pd-TA, ~ 0.91 for Pd-HTA and ~0.87 for Pd-750, respectively. Among those samples, Pd-TA exhibits the largest NO storage capacity (94.1 umol/g) in the presence of CO. It is worth noting that the Pd-SSZ-13 samples contained a certain amount of PdO_x nanoparticles with a very small amount of PdO_2 according to results of H_2-TPR and XPS (Fig. 5). Moreover, PdO nanoparticle in Pd-SSZ-13 have difficulty adsorbing NO even in the presence of CO [7,45]. It is worth noting that the NO/Pd_{ions} ratios of Pd-750, Pd-TA and Pd-HTA in the presence of CO are estimated as 1.30, 1.27 and 1.13, respectively, higher than the theoretical value of ~1. Here, we speculate two possibilities for the additional NO storage of Pd-SSZ-13 in the presence of CO: (1) some Pd^{2+} sites can store two or more NO, such as dinitrosyl species $Pd^{2+}(NO)_2$ [7]; (2) the formation of small amounts of nitrites/nitrates on the zeolites.

Moreover, unlike the two distinct LT and HT NO desorption features in Fig. 6(a), the NO-TPD profiles of Pd-TA and Pd-HTA after NO adsorption with CO exhibited a relatively broad feature from 200 to 500 °C, as shown in Fig. 7. The maximum NO desorption was observed at ~385 °C. Compared with Pd-TA and Pd-HTA, CO had less effect on the NO desorption features of Pd-750, which still showed relatively sharp and narrow desorption peaks from 300 to 400 °C and reached the maximum desorption at ~345 °C. It is proposed that Z-$[Pd^{2+}(OH)]^+$ in Pd-SSZ-13 can be easily reduced to Pd^+ by CO, and store NO as Pd^+-NO, according to the overall reaction R(9) [16,22,41]. The occurrence of the reduction of Pd^{2+} to Pd^+ can be confirmed by the production of CO_2 during the NO_x uptake stage. (Fig. S5) Therefore, the NO should be mainly stored in the form of Pd^+-NO in Pd-750, which was dominated by Z-$[Pd(OH)]^+$ sites. On the other hand, in theory, the Pd^{2+} ions bound to paired Al (Z_2-Pd^{2+}) cannot be reduced by CO [21]. For Pd-TA and Pd-HTA, which contained rather large amounts of Z^{2+}-$[Pd(OH)]^+$ and Z_2-Pd^{2+} sites, the NO adsorption species in the presence of CO and H_2O are more complicated. It has been reported that $Pd^{2+}(NO)(CO)$ complexes and H_2O-solvated Pd-nitrosyl (e.g.$Pd^{2+}(NO)(H_2O)_3$) could possibly be formed on Z_2-Pd^{2+} sites [19,35]. However, no CO or CO_2 could be detected during the TPD stage in our work; thus, the formation of $Pd^{2+}(NO)(CO)$ can be excluded under these conditions. (Fig. S5) Taking the above results into account, the broad NO desorption features of Pd-TA and Pd-HTA are attributed to the multiple Pd^{2+} sites in those two samples, via formation of Pd^+-NO, Pd^{2+}-NO and H_2O-solvated Pd-nitrosyl [14,22,36].

$$2Z\text{-}[Pd(OH)]^+ + 2NO + CO \rightarrow 2Z\text{-}Pd^+\text{-NO} + CO_2 + H_2O \quad (9)$$

Furthermore, PNA experiments were conducted on Pd-750 and Pd-TA to further study the role of Pd sites in NO storage and release. Typically, the NO_x trapping and the subsequent TPD stage are conducted in the same gas flow during PNA experiments. As shown by the results in Fig. 8, the NO_x trapping started at t = 0 min, and then at t = 10 min, TPD from 120 °C to 700 °C was started with a heating rate of 10 °C/min. It seems that the NO_x release from Pd-SSZ-13 under reaction gas flow is similar to the NO_x-TPD process, where Pd-TA exhibits broad NO desorption features from 200 to 400 °C, while the majority of NO_x desorption from Pd-750 appears at higher temperatures above 300 °C. It should be noted that a second NO_x adsorption was found during the desorption stage, exhibiting a negative peak in the temperature range of 120 °C to 220 °C. This might be attributed to the recovery of NO adsorbed sites (such as Pd-hydrate ions) which were inhibited by H_2O at 120 °C [9,41]. In the absence of CO, NO_2 formed immediately after exposure of the catalyst to the reaction gas flow, and then a second NO_2 formation could be observed at the start of heating, resulting from reactions such as R(6) and/or NO oxidation by PdO_x as R(8) [9]. The catalytic oxidation of NO to NO_2 on Pd-SSZ-13 contributes the NO_2 produced at temperatures above 300 °C. Pd-750 exhibits higher NO oxidation activity than Pd-TA, in accordance with the greater amount of PdO species in the former. Fig. 8(b) shows the NO_x trapping and release during PNA experiments in the presence of CO. In this case, the second NO_x adsorption was negligible. This suggests that the inhibition of NO adsorption by H_2O can be eliminated by CO [19,20]. Additionally, the NO adsorption rate was improved in the presence of CO, so that the NO uptake could be completed in ~300 s. This is important to the practical application of PNA materials in NO_x trapping during the first several hundred seconds of cold start.

In order to further understand the effect of CO on Pd species, a Pd-SSZ-13 sample was prepared by using hydrothermally aged H-SSZ-13 as support (denoted as Pd/HTA-SSZ-13). The preparation details and characterization results are shown in the supporting information. In this sample, the majority of Pd are PdO_x particles with the average particle size of 2.8 ± 0.5 nm on the external surface of the crystal, due to just a

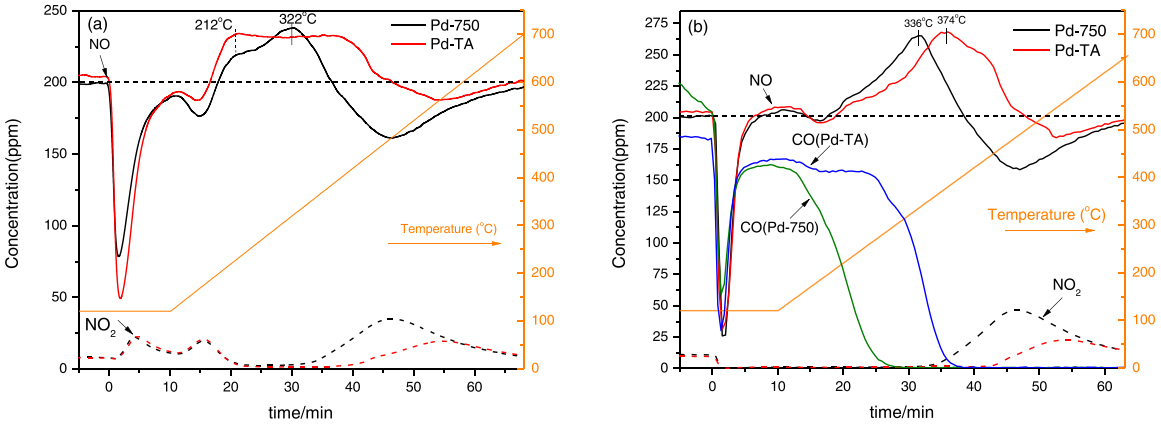

Fig. 8. NO_x uptake/release profiles of Pd-750 and Pd-TA during PNA experiments:(a) 200 ppm NO, 5% H_2O, 10%O_2, N_2 balance, GHSV = 150,000 h^{-1}, (b) 200 ppm NO, ~200 ppm CO, 5%H_2O, 10% O_2, N_2 balance, GHSV = 150,000 h^{-1}.

few ion-exchanged sites remaining in this hydrothermally aged support (Fig. S6). According to H_2-TPR (Fig. S6(c)), the PdO and isolated Pd^{2+} ions in Pd/HTA-SSZ-13 are estimated as ~ 47.0 umol/g and ~ 17.8 umol/g, respectively. As shown by the results in Fig. 9, it was found that the NO adsorption capacities obtained in the absence and presence of CO were very close (~15.0 umol/g), but the desorption features were different. In the absence of CO, most of the stored NO_x was desorbed below 300 °C, according to NO:$NO_2 \approx 2:1$ (Fig. 9(b)). This indicates that the NO/NO_2 desorption resulted from same stored species. Moreover, the low NO storage capacity of Pd/HTA-SSZ-13 suggests that NO storage by PdO via $PdO + NO + 0.5O_2 \rightarrow Pd(NO_3)$ should be difficult under this condition. Therefore, it is reasonable to deduce that the NO_x desorption might be attributed to the decomposition of nitrates or nitrites stored on the zeolites, via $3NO_3^- \rightarrow 2NO + NO_2 + 2.5O_2$or $3NO_2^- \rightarrow 2NO + NO_2 + O_2$. On the other hand, in the presence of CO, the NO_x desorption almost completely consisted of NO, and reached maximum desorption above 300 °C. This suggests that NO could be primarily stored as Pd-nitrosyl, and the NO desorption capacity is ~13 umol/g (NO/Pd_{ions} is ~0.92). The results for Pd/HTA-SSZ-13 further confirm that the inhibition of NO adsorption on Pd^{2+} ions by H_2O can be eliminated by the presence of CO. Moreover, no NO_2 release could be detected below 300 °C. This indicates that the formation of nitrites/nitrates on the zeolite was suppressed by CO.

4. Conclusion

In this work, Pd-SSZ-13 catalysts with highly dispersed Pd^{2+} ions were successfully prepared by both thermal aging and hydrothermal aging treatments at 750 °C for 24 h. Overall, the thermal treatment could be a superior method to realize highly dispersed Pd in zeolites, due to less degradation of the zeolite framework. This study shows that during thermal treatment, the large PdO_x particles and hydrated Pd species(e.g. $Pd(OH)_2$) in the initial Pd-SSZ-13(Pd-500) product were first transformed to small PdO nanoparticles, then dispersed as ion-exchanged Pd^{2+} ions. In particular, Z-$[Pd^{2+}(OH)]^+$ species were preferentially formed, and thermal treatment for a longer time could increase the amount of Z_2-Pd^{2+} species. Furthermore, the Brønsted acid sites in the zeolites participated in the reactions related to re-distribution of Pd species.

The primary NO storage sites in Pd-SSZ-13 are isolated Pd ions (Z-$[Pd^{2+}(OH)]^+$ and Z_2-Pd^{2+} sites), which exhibited two distinct NO desorption features in the 150–300 °C and 300–450 °C regions, respectively. This can be explained as arising from the formation of Pd-nitrosyl complexes with different binding strengths. Moreover, NO adsorption on isolated Pd ions was partially suppressed by H_2O. The presence of CO could eliminate the inhibition of NO adsorption by H_2O, mainly due to the reduction of Pd^{2+} to Pd^+, and realize the full utilization of Pd ions as NO storage sites in the co-existence of CO and H_2O. Although Pd-SSZ-13 contained multiple Pd species, Pd-nitrosyl

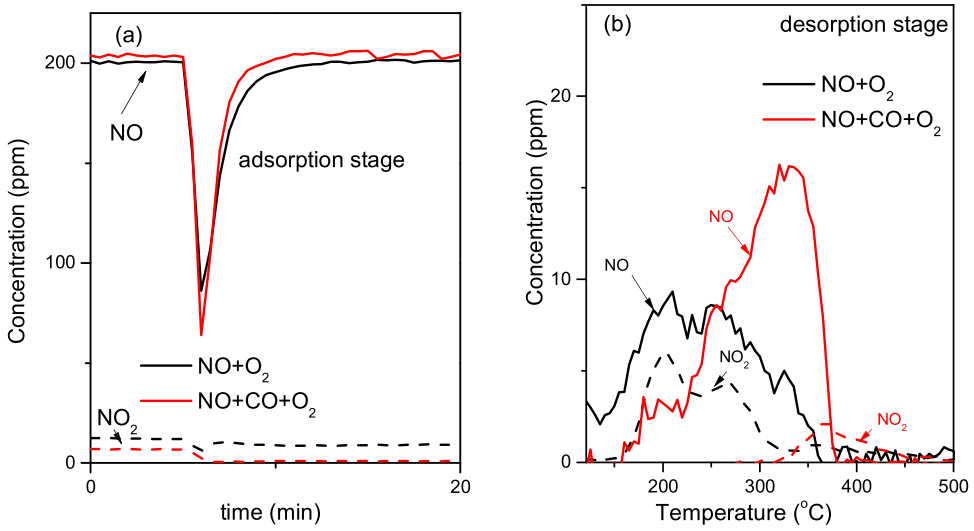

Fig. 9. NO/NO_2 uptake/release profiles of Pd/HTA-SSZ-13: (a) adsorption stage of TPD experiments, (b) desorption stage of TPD experiments.

complexes were predominantly formed in the co-existence of CO and H_2O, from which NO desorbed at 250–450 °C. Additionally, nitrite/nitrate species adsorbed on the zeolite framework can also contribute to the NO adsorption capacity of Pd-SSZ-13, while the presence of CO decreased the formation of those species.

CRediT authorship contribution statement

Yingjie Wang: Conceptualization, Methodology, Investigation, Data curation, Formal analysis, Writing – original draft. **Xiaoyan Shi**: Conceptualization, Methodology, Writing – original draft, Writing – review & editing, Resources, Supervision, Project administration, Funding acquisition. **Zhongqi Liu**: Methodology, Formal analysis, Investigation. **Yulong Shan**: Writing – review & editing, Supervision, Funding acquisition. **Wei Shi**: Methodology, Formal analysis, Investigation. **Yunbo Yu**: Validation, Investigation, Supervision, Visualization. **Hong He**: Conceptualization, Methodology, Writing – review & editing, Resources, Supervision, Funding acquisition.

Declaration of Competing Interest

The authors declare that they have no known competing financial interests or personal relationships that could have appeared to influence the work reported in this paper.

Data availability

Data will be made available on request.

Acknowledgments

This work was financially supported by the National Natural Science Foundation of China (22076206), the Key Project of National Natural Science Foundation Natural Science Foundation (22188102), the National Natural Science Foundation of China (22072179) , Special Project of Eco-environmental Technology for Peak Carbon Dioxide Emissions and Carbon Neutrality (RCEES-TDZ-2021–2).

Appendix A. Supporting information

Supplementary data associated with this article can be found in the online version at doi:10.1016/j.apcatb.2022.122254.

References

[1] J. Lee, J.R. Theis, E.A. Kyriakidou, Vehicle emissions trapping materials: Successes, challenges, and the path forward, Appl. Catal. B 243 (2019) 397–414.
[2] S. Rao, J. Sarlashkar, S. Rengarajan, C. Sharp, G. Neely, A controls overview on achieving ultra-low NO_x, SAE Tech. Pap. Ser. (2020).
[3] S. Bai, J. Han, M. Liu, S. Qin, G. Wang, G.-x Li, Experimental investigation of exhaust thermal management on NO_x emissions of heavy-duty diesel engine under the world Harmonized transient cycle (WHTC), Appl. Therm. Eng. 142 (2018) 421–432.
[4] C. Sharp, C.C. Webb, S. Yoon, M. Carter, C. Henry, Achieving Ultra Low NO_x Emissions Levels with a 2017 Heavy-Duty On-Highway TC Diesel Engine - Comparison of Advanced Technology Approaches, SAE Int. J. Engines 10 (2017) 1722–1735.
[5] Y. Gu, W.S. Epling, Passive NO_x adsorber: An overview of catalyst performance and reaction chemistry, Appl. Catal., A 570 (2019) 1–14.
[6] H.-Y. Chen, J.E. Collier, D. Liu, L. Mantarosie, D. Durán-Martín, V. Novák, R. R. Rajaram, D. Thompsett, Low temperature NO storage of zeolite supported Pd for low temperature diesel engine emission control, Catal. Lett. 146 (2016) 1706–1711.
[7] K. Khivantsev, N.R. Jaegers, L. Kovarik, J.C. Hanson, F.F. Tao, Y. Tang, X. Zhang, I. Z. Koleva, H.A. Aleksandrov, G.N. Vayssilov, Y. Wang, F. Gao, J. Szanyi, Achieving Atomic Dispersion of Highly Loaded Transition Metals in Small-Pore Zeolite SSZ-13: High-Capacity and High-Efficiency Low-Temperature CO and Passive NO_x Adsorbers, Angew. Chem. Int. Ed. Engl. 57 (2018) 16672–16677.
[8] J. Lee, Y. Ryou, S. Hwang, Y. Kim, S.J. Cho, H. Lee, C.H. Kim, D.H. Kim, Comparative study of the mobility of Pd species in SSZ-13 and ZSM-5, and its implication for their activity as passive NO_x adsorbers (PNAs) after hydro-thermal aging, Catal. Sci. Technol. 9 (2019) 163–173.
[9] Y. Zheng, L. Kovarik, M.H. Engelhard, Y. Wang, Y. Wang, F. Gao, J. Szanyi, Low-Temperature Pd/Zeolite Passive NO_x Adsorbers: Structure, Performance, and Adsorption Chemistry, J. Phys. Chem. C. 121 (2017) 15793–15803.
[10] J. Lee, Y. Ryou, S.J. Cho, H. Lee, C.H. Kim, D.H. Kim, Investigation of the active sites and optimum Pd/Al of Pd/ZSM–5 passive NO adsorbers for the cold-start application: Evidence of isolated-Pd species obtained after a high-temperature thermal treatment, Appl. Catal. B 226 (2018) 71–82.
[11] P. Kim, J. Van der Mynsbrugge, H. Aljama, T.M. Lardinois, R. Gounder, M. Head-Gordon, A.T. Bell, Investigation of the modes of NO adsorption in Pd/H-CHA, Appl. Catal. B 304 (2022) 120992–121005.
[12] J. Van der Mynsbrugge, M. Head-Gordon, A.T. Bell, Computational Modeling Predicts the Stability of Both Pd^+ and Pd^{2+} Ion-Exchanged into H-CHA, J. Mater. Chem. A 9 (2021) 2161–2174.
[13] Y. Ryou, J. Lee, S.J. Cho, H. Lee, C.H. Kim, D.H. Kim, Activation of Pd/SSZ-13 catalyst by hydrothermal aging treatment in passive NO adsorption performance at low temperature for cold start application, Appl. Catal. B 212 (2017) 140–149.
[14] H. Zhao, X. Chen, A. Bhat, Y. Li, J.W. Schwank, Understanding the chemistry during the preparation of Pd/SSZ-13 for the low-temperature NO adsorption: The role of NH_4-SSZ-13 support, Appl. Catal. B 282 (2021) 119611–119619.
[15] S. Yasumura, H. Ide, T. Ueda, Y. Jing, C. Liu, K. Kon, T. Toyao, Z. Maeno, K. I. Shimizu, Transformation of Bulk Pd to Pd Cations in Small-Pore CHA Zeolites Facilitated by NO, JACS Au 1 (2021) 201–211.
[16] J. Lee, J. Kim, Y. Kim, S. Hwang, H. Lee, C.H. Kim, D.H. Kim, Improving NO_x storage and CO oxidation abilities of Pd/SSZ-13 by increasing its hydrophobicity, Appl. Catal. B 277 (2020) 119190–119202.
[17] T.M. Lardinois, J.S. Bates, H.H. Lippie, C.K. Russell, J.T. Miller, H.M. Meyer, K. A. Unocic, V. Prikhodko, X. Wei, C.K. Lambert, A.B. Getsoian, R. Gounder, Structural Interconversion between Agglomerated Palladium Domains and Mononuclear Pd(II) Cations in Chabazite Zeolites, Chem. Mater. 33 (2021) 1698–1713.
[18] K. Khivantsev, X. Wei, L. Kovarik, N.R. Jaegers, E.D. Walter, P. Tran, Y. Wang, J. Szanyi, Palladium/Ferrierite versus Palladium/SSZ-13 Passive NO_x Adsorbers: Adsorbate-Controlled Location of Atomically Dispersed Palladium(II) in Ferrierite Determines High Activity and Stability, Angew. Chem. Int. Ed. Engl. 61 (2022), e202107554.
[19] K. Khivantsev, F. Gao, L. Kovarik, Y. Wang, J. Szanyi, Molecular Level Understanding of How Oxygen and Carbon Monoxide Improve NO_x Storage in Palladium/SSZ-13 Passive NO_x Adsorbers: The Role of NO^+ and Pd(II)(CO)(NO,) Species, J. Phys. Chem. C. 122 (2018) 10820–10827.
[20] I. Song, K. Khivantsev, Y. Wang, J. Szanyi, Elucidating the Role of CO in the NO Storage Mechanism on Pd/SSZ-13 with in Situ DRIFTS, J. Phys. Chem. C. 126 (2022) 1439–1449.
[21] A. Vu, J. Luo, J. Li, W.S. Epling, Effects of CO on Pd/BEA Passive NO_x Adsorbers, Catal. Lett. 147 (2017) 745–750.
[22] A. Gupta, S.B. Kang, M.P. Harold, NO_x uptake and release on Pd/SSZ-13: Impact Of Feed composition and temperature, Catal. Today 360 (2021) 411–425.
[23] D. Yao, R.F. Ilmasani, J.C. Wurzenberger, T. Glatz, J. Han, P.H. Ho, D. Creaser, L. Olsson, Insight into CO induced degradation mode of Pd/SSZ-13 in NO_x adsorption and release: Experiment and modeling, Chem. Eng. J. 439 (2022) 135714–135727.
[24] H. Zhao, X. Chen, A. Bhat, Y. Li, J.W. Schwank, Insight into hydrothermal aging effect on deactivation of Pd/SSZ-13 as low-temperature NO adsorption catalyst: Effect of dealumination and Pd mobility, Appl. Catal. B 286 (2021) 119874–119888.
[25] A. Wang, K. Lindgren, M. Di, D. Bernin, P.-A. Carlsson, M. Thuvander, L. Olsson, Insight into hydrothermal aging effect on Pd sites over Pd/LTA and Pd/SSZ-13 as PNA and CO oxidation monolith catalysts, Appl. Catal. B 278 (2020), 119315-111928.
[26] F. Gao, Y. Wang, N.M. Washton, M. Kollár, J. Szanyi, C.H.F. Peden, Effects of Alkali and Alkaline Earth Cocations on the Activity and Hydrothermal Stability of Cu/SSZ-13 NH_3–SCR Catalysts, ACS Catal. 5 (2015) 6780–6791.
[27] S. Li, A. Zheng, Y. Su, H. Zhang, L. Chen, J. Yang, C. Ye, F. Deng, Brønsted/Lewis Acid Synergy in Dealuminated HY Zeolite: A Combined Solid-State NMR and Theoretical Calculation Study, J. Am. Chem. Soc. 129 (2007) 11161–11171.
[28] D.W. Fickel, R.F. Lobo, Copper Coordination in Cu-SSZ-13 and Cu-SSZ-16 Investigated by Variable-Temperature XRD, J. Phys. Chem. C. 114 (2010) 1633–1640.
[29] Z. Chen, M. Wang, J. Wang, C. Wang, J. Wang, W. Li, M. Shen, Investigation of crystal size effect on the NO_x storage performance of Pd/SSZ-13 passive NO_x adsorbers, Appl. Catal. B 291 (2021) 120026–120036.
[30] D. Chen, H. Lei, W. Xiong, Y. Li, X. Ji, J.-Y. Yang, B. Peng, M. Fu, P. Chen, D. Ye, Unravelling Phosphorus-Induced Deactivation of Pd-SSZ-13 for Passive NO_x Adsorption and CO Oxidation, ACS Catal. 11 (2021) 13891–13901.
[31] Y. Cui, J. Zhu Chen, B. Peng, L. Kovarik, A. Devaraj, Z. Li, T. Ma, Y. Wang, J. Szanyi, J.T. Miller, Y. Wang, F. Gao, Onset of high methane combustion rates over supported palladium catalysts: from isolated Pd cations to PdO nanoparticles, JACS Au 1 (2021) 396–408.
[32] Y. Lou, J. Ma, W. Hu, Q. Dai, L. Wang, W. Zhan, Y. Guo, X.-M. Cao, Y. Guo, P. Hu, G. Lu, Low-Temperature Methane Combustion over Pd/H-ZSM-5: Active Pd Sites with Specific Electronic Properties Modulated by Acidic Sites of H-ZSM-5, ACS Catal. 6 (2016) 8127–8139.
[33] H. Hosseiniamoli, G. Bryant, E.M. Kennedy, K. Mathisen, D. Nicholson, G. Sankar, A. Setiawan, M. Stockenhuber, Understanding Structure–Function Relationships in Zeolite-Supported Pd Catalysts for Oxidation of Ventilation Air Methane, ACS Catal. 8 (2018) 5852–5863.

[34] A.A. Gabrienko, I.G. Danilova, S.S. Arzumanov, L.V. Pirutko, D. Freude, A. G. Stepanov, Direct Measurement of Zeolite Brønsted Acidity by FTIR Spectroscopy: Solid-State ^{1}H MAS NMR Approach for Reliable Determination of the Integrated Molar Absorption, Coeff., J. Phys. Chem. C. 122 (2018) 25386–25395.
[35] A.W. Petrov, D. Ferri, O. Kröcher, J.A. van Bokhoven, Design of stable palladium-based zeolite catalysts for complete methane oxidation by postsynthesis zeolite modification, ACS Catal. 9 (2019) 2303–2312.
[36] K. Mandal, Y. Gu, K.S. Westendorff, S. Li, J.A. Pihl, L.C. Grabow, W.S. Epling, C. Paolucci, Condition-Dependent Pd Speciation and NO Adsorption in Pd/Zeolites, ACS Catal. 10 (2020) 12801–12818.
[37] M.-C. Silaghi, C. Chizallet, P. Raybaud, Challenges on molecular aspects of dealumination and desilication of zeolites, Microporous Mesoporous Mater. 191 (2014) 82–96.
[38] D. Mei, F. Gao, J. Szanyi, Y. Wang, Mechanistic insight into the passive NO_x adsorption in the highly dispersed Pd/HBEA zeolite, Appl. Catal., A 569 (2019) 181–189.
[39] B.J. Adelmana, W.M.H. Sachtler, The effect of zeolitic protons on NO_x reduction over Pd/ZSM-5 catalysts, Appl. Catal. B 14 (1997) 1–11.
[40] J. Song, Y. Wang, E.D. Walter, N.M. Washton, D. Mei, L. Kovarik, M.H. Engelhard, S. Prodinger, Y. Wang, C.H.F. Peden, F. Gao, Toward rational design of Cu/SSZ-13 selective catalytic reduction catalysts: implications from atomic-level understanding of hydrothermal stability, ACS Catal. 7 (2017) 8214–8227.
[41] R. Villamaina, U. Iacobone, I. Nova, E. Tronconi, M.P. Ruggeri, L. Mantarosie, J. Collier, D. Thompsett, Mechanistic insight in NO trapping on Pd/Chabazite systems for the low-temperature NO_x removal from Diesel exhausts, Appl. Catal. B 284 (2020) 119724–119736.
[42] M. Ambast, K. Karinshak, B.M.M. Rahman, L.C. Grabow, M.P. Harold, Passive NO_x adsorption on Pd/H-ZSM-5: Experiments and modeling, Appl. Catal. B 269 (2020) 118802–118817.
[43] I. Song, K. Khivantsev, Y. Wu, M. Bowden, Y. Wang, J. Szanyi, Unusual water-assisted NO adsorption over Pd/FER calcined at high temperatures: The effect of cation migration, Appl. Catal. B 318 (2022).
[44] Y. Gu, S. Sinha Majumdar, J.A. Pihl, W.S. Epling, Investigation of NO adsorption and desorption phenomena on a Pd/ZSM-5 passive NO_x adsorber, Appl. Catal. B 298 (2021).
[45] Y. Ryou, J. Lee, Y. Kim, S. Hwang, H. Lee, C.H. Kim, D.H. Kim, Effect of reduction treatments (H_2 vs. CO) on the NO adsorption ability and the physicochemical properties of Pd/SSZ-13 passive NO_x adsorber for cold start application, Appl. Catal., A 569 (2019) 28–34.
[46] Y. Gu, R.P. Zelinsky, Y.-R. Chen, W.S. Epling, Investigation of an irreversible NO_x storage degradation Mode on a Pd/BEA passive NO_x adsorber, Appl. Catal. B 258 (2019) 118032–118040.